Stability and carrier transport properties of phosphorene-based polymorphic nanoribbons

To cite this article: Sumandeep Kaur *et al* 2018 *Nanotechnology* **29** 155701

View the article online for updates and enhancements.

Related content

- Quantum confinement in black phosphorus-based nanostructures
  Andrew Cupo and Vincent Meunier

- The structure and elastic properties of phosphorene edges
  V Sorkin and Y W Zhang

- Effects of edge reconstruction on the common groups terminated zigzag phosphorene nanoribbon
  Huaping Xiao, Sumei Guo, Chunxiao Zhang et al.
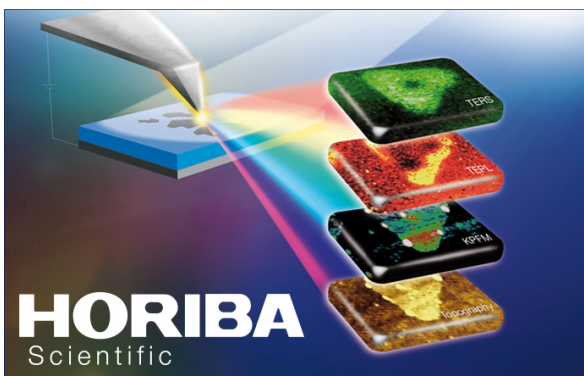
Stability and carrier transport properties of phosphorene-based polymorphic nanoribbons

Sumandeep Kaur[1,2] ⊙**, Ashok Kumar**[2,5] ⊙**, Sunita Srivastava**[1] ⊙**, Ravindra Pandey**[3] ⊙ **and K Tankeshwar**[1,4,5]

[1] Department of Physics, Panjab University, Chandigarh 160014, India
[2] Department of Physical Sciences, School of Basic and Applied Sciences, Central University of Punjab, Bathinda, 151001, India
[3] Department of Physics, Michigan Technological University, Houghton, MI, 49931, United States of America
[4] Department of Physics, Guru Jambheshwar University of Science and Technology, Hisar, 125001, Haryana, India

E-mail: ashokphy@cup.edu.in and tkumar@gjust.org

Abstract

Few-layer black phosphorene has recently attracted significant interest in the scientific community. In this paper, we consider several polymorphs of phosphorene nanoribbons (PNRs) and employ deformation potential theory within the effective mass approximation, together with density functional theory, to investigate their structural, mechanical and electronic properties. The results show that the stability of a PNR strongly depends on the direction along which it can be cut from its 2D counterpart. PNRs also exhibit a wide range of line stiffnesses ranging from $6 \times 10^{10} \, \text{eV m}^{-1}$ to $18 \times 10^{11} \, \text{eV m}^{-1}$, which has little dependence on the edge passivation. Likewise, the calculated electronic properties of PNRs show them to be either a narrow-gap semiconductor ($E_\text{g} < 1 \, \text{eV}$) or a wide-gap semiconductor ($E_\text{g} > 1 \, \text{eV}$). The carrier mobility of PNRs is found to be comparable to that of black phosphorene. Some of the PNRs show an n-type (p-type) semiconducting character owing to their higher electron (hole) mobility. Passivation of the edges leads to n-type ↔ p-type transition in many of the PNRs considered. The predicted novel characteristics of PNRs, with a wide range of mechanical and electronic properties, make them potentially suitable for use in nanoscale devices.

Supplementary material for this article is available online

Keywords: phosphorene, nanoribbons, polymorphs, density functional theory, carrier mobility

(Some figures may appear in colour only in the online journal)

1. Introduction

Since its successful exfoliation in 2014, few-layer black phosphorene has attracted significant interest in the scientific community [1]. Monolayer black phosphorene (α-P), with its unique anisotropic puckered structure, is a direct band gap semiconductor with a bandgap of ~1.0 eV [2]. It is found to

withstand mechanical strains as high as 40% with a large lateral flexibility [3]. Another equally stable 2D allotrope of phosphorus is blue phosphorene (β-P) which has recently been realized experimentally [4, 5]. Blue phosphorene possesses a graphene-like structure with the out-of-plane buckling of 2.2 Å and an indirect band gap of ~2.0 eV [6]. Both black and blue phosphorene have intrinsic carrier mobility of as high as $10^3 \, \text{cm}^2 \, \text{V}^{-1} \, \text{s}^{-1}$ [7, 8]. The high carrier mobility and semiconducting characteristics of α- and β-P makes them

---

[5] Authors to whom any correspondence should be addressed.

promising materials for application in optical and electronic devices [9].

Bulk phosphorus can form various allotropes such as violet, red, white and black due to the inequivalent sp^3 hybridization of orbitals in the lattice [3]. Likewise, a number of structurally different 2D polymorphs of phosphorous, namely α-P, β-P, γ-P, δ-P, ε-P, τ-P, η-P, θ-P, ϕ-P, tricycle-type red phosphorene (R-P), square-octagon phosphorene (O-P) and hexagonal-star phosphorene (H-P), have been investigated using the first principles method [10–17]. α-P, β-P, γ-P, δ-P and R-P exhibit a buckled honeycomb structure consisting of a six-membered ring similar to graphene, while ε-P, τ-P, η-P, θ-P, ϕ-P, O-P, and H-P crystallize into non-honeycomb structural arrangements. Red phosphorene is constructed by the in-plane connections of the segments of α-P and β-P [14]. ε-P and τ-P consist of squared units of phosphorus atoms while η-P and θ-P have phosphorus atoms in the pentagon structural arrangement [12]. ϕ-P consists of 4, 6 and 10 membered rings [13], and the O-P allotrope contains a unique atomic octagonal tiling (OT) pattern consisting of four and eight membered rings [15]. The phosphorus atoms in H-P form a hexagonal lattice with a Magen–David-like top view [16]. The honeycomb structures of phosphorene exhibit two type of edges i.e., armchair and zigzag, whereas most of the non-honeycomb structures are found to possess more than two distinctly different edges. All these 2D polymorphs are found to be semiconducting in nature with a band gap ranging from 0.4 eV to 2.1 eV [10–17]. Note that α-P and β-P are experimentally realized, whereas the other allotropes are yet to be synthesized.

Similar to 1D graphene nanoribbons (GNRs), the phosphorene 1D nanoribbons can be constructed from their 2D counterpart by cutting along various edge directions. Several 1D structures of black and blue phosphorene have been investigated previously [9]. The α- and β-phosphorene nanoribbons possess two types of edge i.e. armchair (AC) and zigzag (ZZ), which strongly influence their band gaps [18, 19]. External electric field has been shown to modify the electronic band gap of both AC and ZZ α-phosphorene nanoribbons (PNRs) due to the giant stark-effect [20, 21]. Also, the electron/hole effective masses and carrier mobility of both α- and β-PNRs are found to depend on the edge configurations [22]. On the other hand, in the non-honeycomb PNR structures, various types of edge exist and it will be interesting to investigate their properties.

In the present work we consider five honeycomb and eight non-honeycomb phosphorene polymorphs, and report the results of density functional theory calculations to determine energetics, mechanical stability and carrier mobility. In the following, section 2 briefly describes the computational model. Results are discussed in section 3, and a summary is given in section 4.

2. Computational method

Density functional theory calculations were performed using the SIESTA program package [23]. The norm-conserving Troullier–Martin pseudopotential was used to treat the electron–ion interactions [24], whereas the exchange and correlation energies were described using the GGA functional form [25]. A double zeta basis set with polarization functions (DZP) was used to expand the Kohn–Sham orbitals with the mesh cutoff energy of 450 Ry. The minimization of energy was carried out using the conjugate-gradient (CG) technique with the forces less than 0.01 eV Å^{-1} on each atom. The Monkhorst–Pack scheme was used to sample the Brillouin zone with a $(30 \times 30 \times 1)$ mesh for 2D sheets. Meshes of $(30 \times 1 \times 1)$ and $(1 \times 30 \times 1)$ were used for PNRs with lengths along the *x* and *y* directions, respectively. A vacuum region greater than 20 Å along the two directions has been used in calculations to avoid the superficial interactions due to replicas.

$$\mu_{1D} = \frac{e\hbar^2 C_{1D}}{(2\pi k_B T)^{1/2} |m^*|^{3/2} E_1^2}. \tag{1}$$

The carrier transport in PNRs was calculated using deformation potential (DP) theory [26] and effective mass approximation. The lowest energy PNR structures were considered for calculations. For 1D systems, an analytical expression [27] for the mobility (μ) was employed as follows.

$T = 300$ K and m^* is the effective mass of the charge carriers, defined as $m^* = \hbar^2 (\partial^2 E(k)/\partial k^2)^{-1}$. C is the stretching modulus caused by the uniaxial-strain (ε), which has been calculated using the expression $C_{1D} = \frac{1}{L_0} \frac{d^2 E_S}{de^2}$, in which E_S is the strain energy of a unit cell and L_0 is the equilibrium lattice constant. E_1 in equation (1) is the deformation-potential (DP) constant, which denotes the shift of the band-edge energy induced by strain, and has been obtained as $E_1 = \frac{dE_{edge}}{de}$, where E_{edge} is the energy of the conduction band minimum (for electrons) or the valence band maximum (for holes). Note that equation (1) has been successfully applied previously to study the intrinsic mobility of GNRs [28], graphyne nanoribbons [29] and PNRs [9].

3. Results and discussions

Depending upon the ways that tetrahedrally coordinated P-atoms in a 2D lattice are connected, different structural allotropes can be formed. We have considered a number of allotropes of phosphorene, including β-P, γ-P, δ-P, ε-P, τ-P, η-P, θ-P, ϕ-P, κ_4-P, R-P, O-P and H-P. All these allotropes are found to be semiconducting with a calculated band gap varying from 0.48 eV to 2.09 eV (table S1 of ESI is available online at stacks.iop.org/NANO/29/155701/mmedia).

The magnitude of the relative formation energies (E_{RFmono}) of all these 2D allotropes are found to be in the order of 10–10^2 meV/atom, indicating their ease of formation. This suggests that not only the α- and β-P, but the other allotropes, can also be experimentally realized. Hence, it is worth exploring the properties of other allotropes. Note that E_{RFmono} can be obtained as: $E_{RFmono} = \frac{E_A - N E_\alpha}{N}$, where E_A is the total energy of the
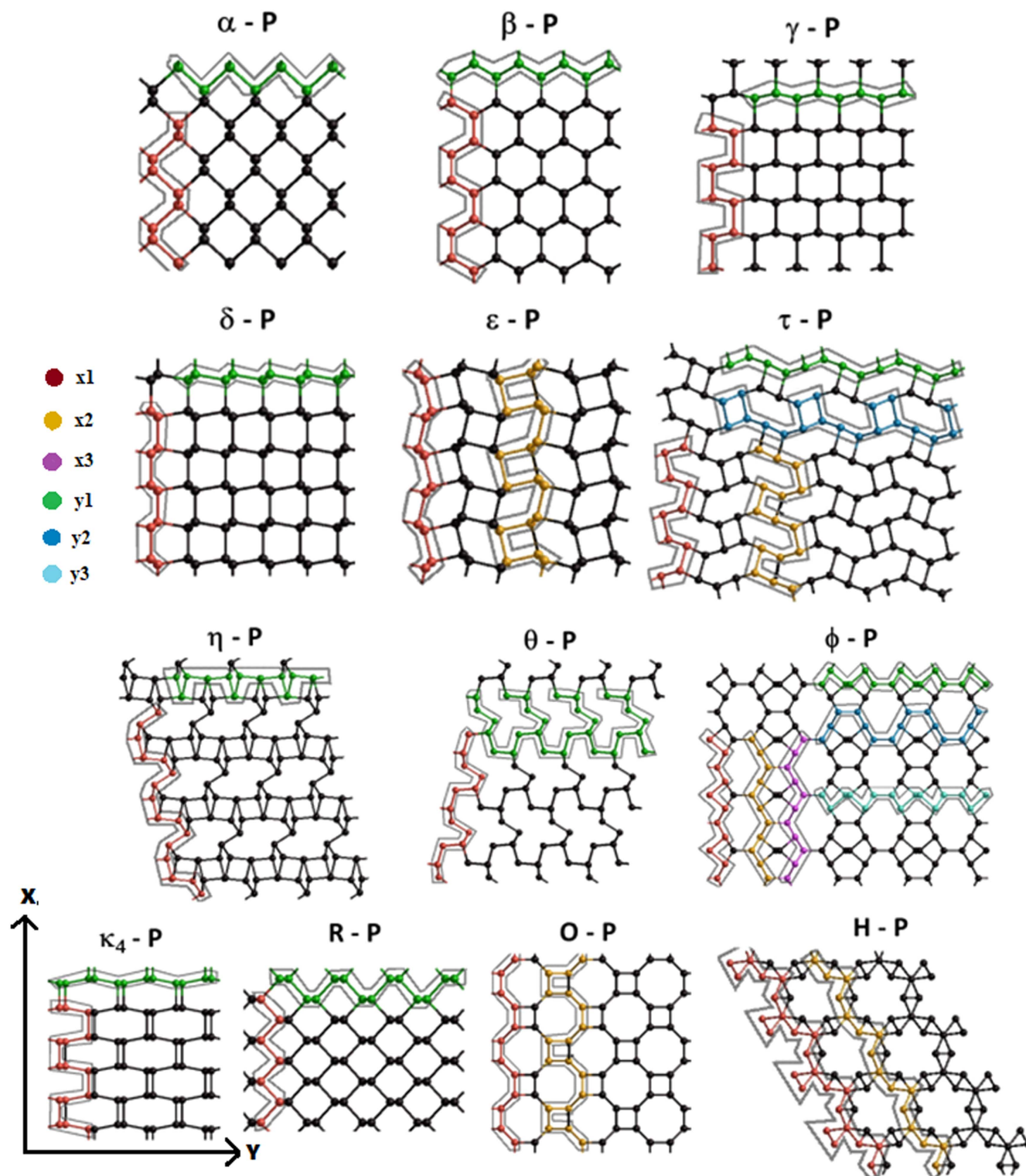
Figure 1. Phosphorene allotropes indicating different types of edge (with different colors) in different directions (*x* and *y*). Since *η*-P and *θ*-P possess a large number of edge structures, a few representative cases are presented here while others are given in figure S1 of ESI.

considered phosphorene allotrope, E_α is the energy per atom of the most stable phosphorene allotrope i.e. *α*-P, and *N* is the number of atoms per unit cell of the allotrope. Similarly, the cohesive energies are in the range of −5.50 to −5.66 eV/atom and are comparable with that of *α*-P (−5.68 eV/atom) (table S1 of ESI).

Figure 1 shows the different types of possible edges of the allotropes of phosphorene considered. Each allotrope cut along the distinct edges gives rise to a distinct phosphorene nanoribbon. The honeycomb structures (*α*-P, *β*-P, *γ*-P, *δ*-P and R-P) possess two edge structures, one along the *x*-direction and the other along the *y*-direction. Unlike these

Table 1. Calculated deformation potential (E_1), energy bandgap of bare and passivated PNRs. (*a*) is length and (*w*) is width along the periodic direction of the bare PNRs.

System	Length (*a*) (Å)	Width (*w*) (Å)	Bare PNR			Passivated PNR		
			E_1 (electrons) (eV)	E_1 (holes) (eV)	E_g (eV)	E_1 (electrons) (eV)	E_1 (holes) (eV)	E_g (eV)
α_{x1}	4.46	18.99	1.35	−1.20	0.37	1.61	−1.5	0.99
β_{x1}	5.81	17.39	4.51	−4.10	1.08	−7.05	0.14	2.20
γ_{x1}	5.40	18.37	3.25	−3.25	0.36	1.86	−1.75	0.71
δ_{x1}	5.39	29.96	3.54	−3.17	0.35	4.34	−4.33	0.41
ε_{x1}	5.40	29.09	−0.70	0.14	0.64	0.76	−0.83	0.57
τ_{x1}	5.33	38.10	−4.97	4.47	0.73	−6.74	2.14	1.27
τ_{y2}	6.53	29.64	−1.08	2.27	1.14	−2.21	0.91	1.27
η_{x3}	6.39	25.39	0.80	−0.66	0.74	2.03	−2.04	0.99
η_{y2}	5.43	33.73	−1.66	1.52	0.85	−3.92	2.41	0.99
θ_{x1}	6.36	31.12	0.46	−0.68	0.16	1.75	−1.74	0.75
θ_{y3}	5.54	30.36	0.05	−0.70	1.08	−0.58	1.58	1.25
ϕ_{x1}	6.20	46.35	−4.03	3.05	0.32	−0.81	0.91	1.03
ϕ_{y3}	7.81	37.53	0.49	−0.56	0.90	−0.91	1.22	1.04
κ_{4x1}	5.52	30.40	4.64	−2.06	0.30	1.81	−1.92	0.39
R_{y1}	8.92	18.96	2.45	−2.40	0.51	−3.12	−9.21	1.26
O_{x2}	6.53	34.71	−4.71	−4.96	1.81	−2.43	−0.62	2.10
H_{x1}	6.27	37.09	2.28	3.81	1.40	1.83	3.44	1.48

honeycomb structures which possess only one type of edge along each direction, the non-honeycomb structures possess more than one different type of edge along different directions. Due to the perfect square symmetry in the unit cell of ε-P and O-P, they possess two different edge structures (ε_{x1}, ε_{x2} and O_{x1}, O_{x2}) along one direction which are also similar in other direction (figure 1). The H-P allotrope also exhibits two types of edge structure (H_{x1} and H_{x2}) along one direction which are also similar in the other direction due to the hexagonal symmetry in its structure. τ-P forms four PNR structures corresponding to the two different types of edge along each direction shown in figure 1. η-P possesses 11 PNR structures, five along the *x*-axis (η_{x1}, η_{x2}, η_{x3}, η_{x4} and η_{x5}) and six along the *y*-axis (η_{y1}, η_{y2}, η_{y3}, η_{y4}, η_{y5} and η_{y6}) (figures 1 & S1 of ESI). θ-P possesses seven PNRs structures, four along the *x*-axis (θ_{x1}, θ_{x2}, θ_{x3} and θ_{x4}) and three along the *y*-axis (θ_{y1}, θ_{y2} and θ_{y3}). ϕ-P forms six PNR structures, three along the *x*-axis (ϕ_{x1}, ϕ_{x2}, and ϕ_{x3}) and three along the *y*-axis (ϕ_{y1}, ϕ_{y2} and ϕ_{y3}). κ_4-P possesses two different structures, one along each direction (κ_{4x1} and κ_{4y1}). The width of the considered PNRs lies in the range 17 Å to 46 Å (table 1).

Therefore, depending on the edge configuration in the *x*- and *y*-directions, a total of 46 structures (figures 1, S1 and S2 of ESI) were considered. Note that in the equilibrium configurations, the edge atoms in the bare PNRs show reconstruction due to the presence of the dangling bonds (figure S2 of ESI). The dangling bonds on the edges of a given PNR are then terminated by hydrogen atoms (figure S3).

3.1. Structural stability

In order to study the energetic stability of the considered PNRs, we have calculated their formation energy (E_{FPNR})

which is defined as the energy required to form these nanoribbons from their 2D counterpart. The formula is given as: $E_{FPNR} = \frac{E_R - NE_{2D}}{N}$, where E_R is the total energy of the ribbons, E_{2D} is the energy per atom of the 2D sheet and *N* is the number of atoms per unit cell of the ribbons. The E_{FPNR} for ribbons (except β-PNRs) are found to be lower than that of the black phosphorene nanoribbons (α-PNRs), thereby indicating these PNRs to be energetically more favorable than the PNRs of the most stable black phosphorus.

The energetic stability of PNRs are found to be strongly dependent on the direction along which they can be cut from their 2D counterpart. It is found that four of the 2D monolayer structures (i.e. β-P, η-P, θ-P and R-P) have a formation energy comparable (the energy difference being less than 40 meV/atom) with the most stable monolayer structure (α-P) (figures 2(a) and (b)), indicating that these monolayers are equally stable. Other 2D structures are energetically not favorable, however, their 1D counterparts show energetically favorable structures which is evident from their low value formation energies. Note that β-P, η-P, θ-P, R-P and H-P possess the least tension in their structures due to the presence of either five or six membered rings, whereas the increased tension in ε-P, τ-P, ϕ-P, κ_4-P and O-P due to the presence of four membered rings in their structures, makes them less favorable. However, the energy difference of the order of a few meV indicates their ease of formation.

In order to obtain a greater insight into the energetics of the given PNRs structures, the binding energy was calculated using the formula: $E_B = \frac{E_R - NE_S}{N}$, where E_R is the total energy of the ribbon, E_S is the energy of the isolated single phosphorene atom and *N* is the number of atoms in the ribbon. The binding energies of the PNRs lay within the range −5.65 to 15.45 eV/atom (figures 2(c) and (d)) which are comparable to
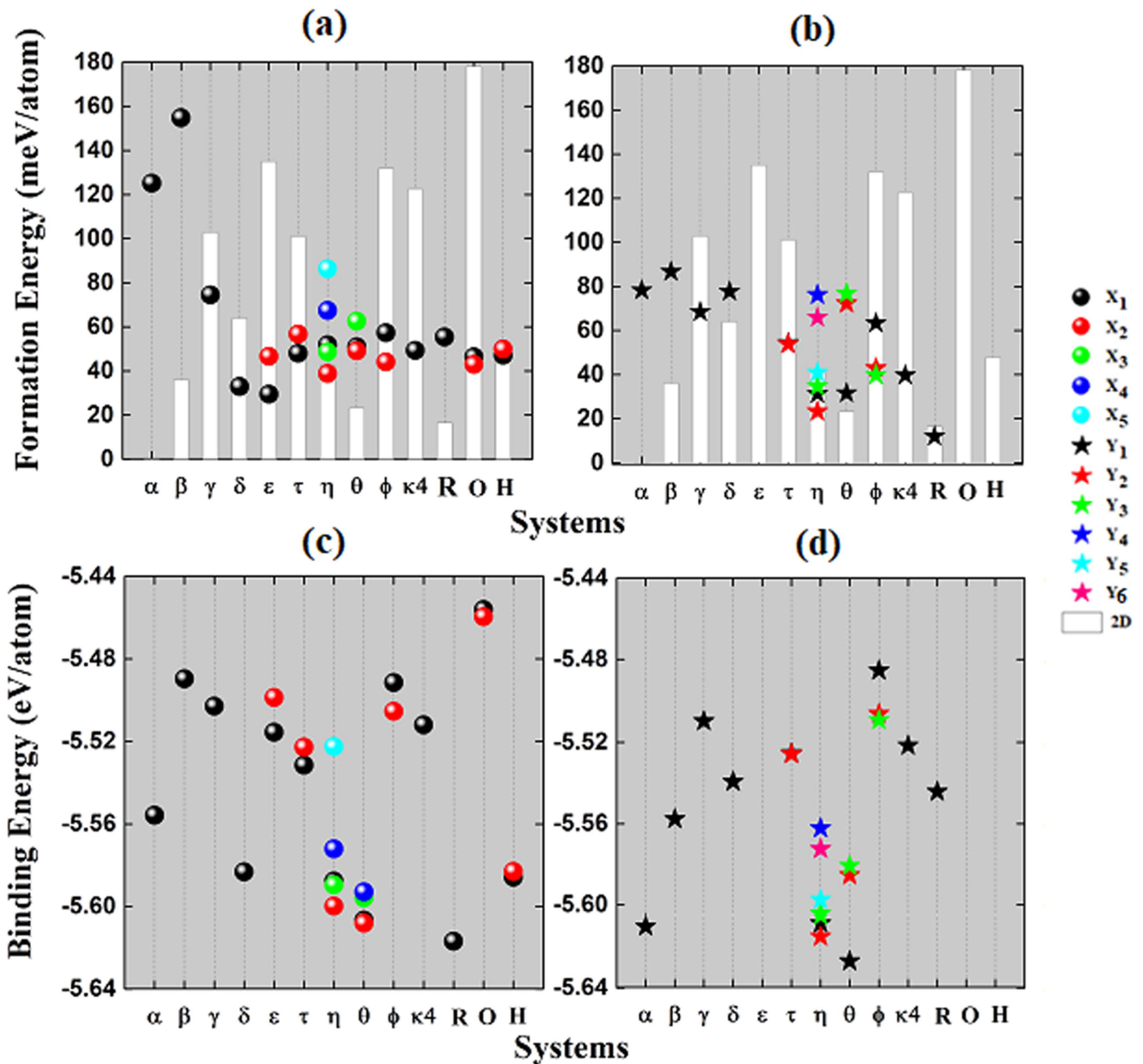
Figure 2. Formation energy per atom and binding energy per atom of the PNRs considered. The bars in (a) and (b) shows the data for the 2D sheet.

the binding energy (-5.68 eV/atom) of the most stable black phosphorene monolayer.

3.2. Mechanical properties

The representative structures in each edge direction, based on the minimum total energy criterion, were considered in order to determine their mechanical property, which led to a total of 34 semiconducting (17 bare and 17 passivated) PNRs. The stiffness of a material is an important parameter in describing its mechanical stability. The stiffer an object is, the less flexible it is. In 1D ribbons one can calculate line stiffness using the formula: $C_{1D} = \frac{1}{L_0} \frac{d^2 E_S}{de^2}$, where E_S is the difference between the total energy of the equilibrium and the strained PNRs, e is the applied strain and L_0 is the length

of the ribbon. For each ribbon, a strain varying from -1% to $+1\%$ in steps of 0.5% is applied along the length of the ribbon. The line stiffness is then calculated by fitting the strained energy (E_S) versus strain (e) curve with the formula $E_S = a_0 e^2 + a_1 e + a_2$ (figures 3(a), (b) and S4).

It is found that the line stiffness of PNRs varies from 6×10^{10} eV m^{-1} (for R_{y1}-PNR) to 18.6×10^{11} eV m^{-1} (for ϕ_{x1}-PNR) (figure 3) indicating that an R-PNR cut along the y-direction is most flexible while a ϕ-P cut along the x-direction is the least flexible. Note that the calculated value of α-PNR is 16.6×10^{10} eV m^{-1}. Line stiffness depends upon the inverse of the length of the nanoribbon, which is not affected by passivation. Also, the strain is applied in the small region i.e. $\pm 1\%$ where Hook's law is applicable. The rate of change of energy with strain for the passivated and unpassivated PNRs
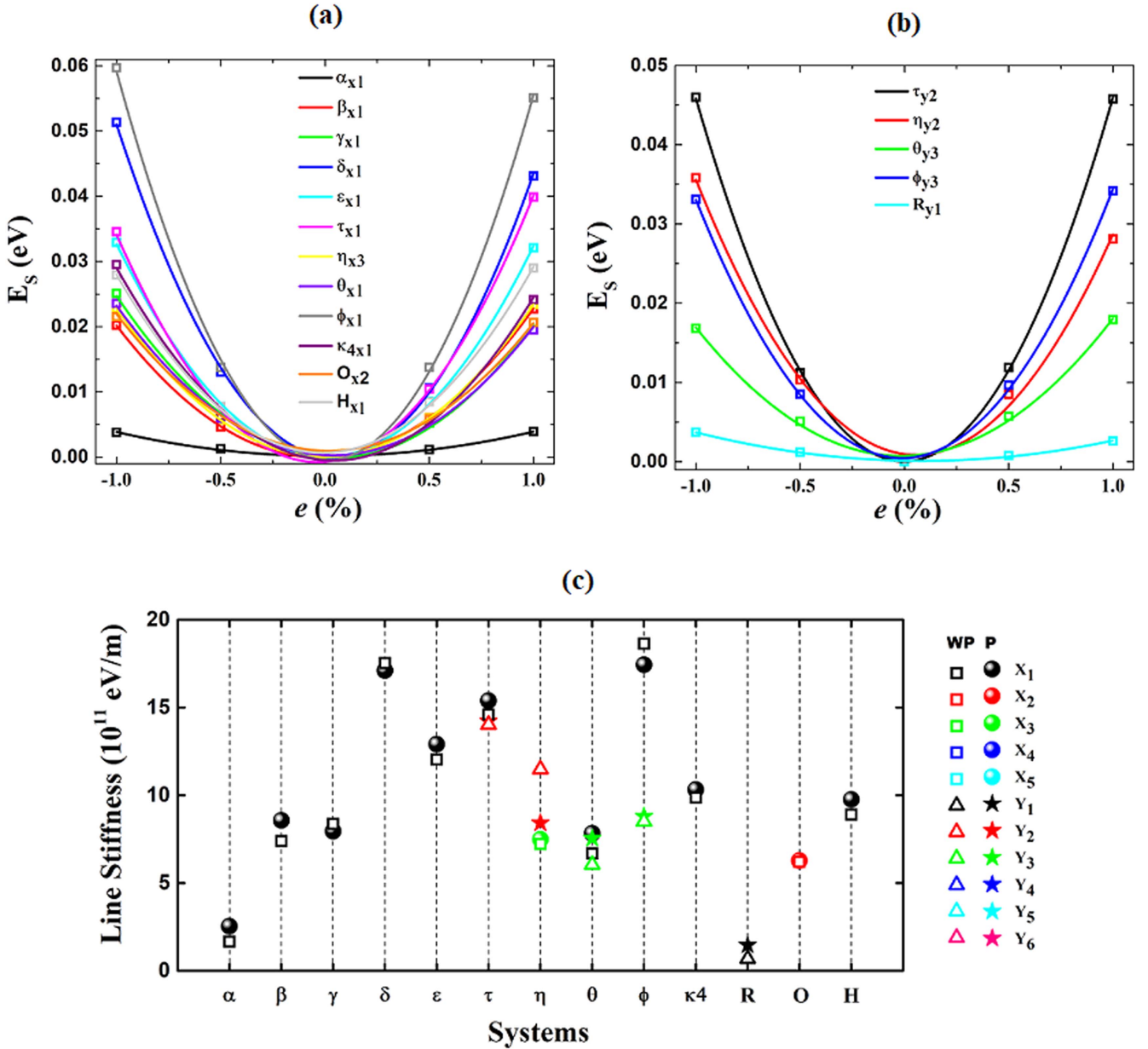
Figure 3. (Top) Bare PNRs: strain energy versus strain applied along the (a) *x*-axis, and (b) *y*-axis. (Bottom) (c) The line stiffness of bare (WP) and passivated (P) PNRs considered.

remains nearly identical, which leads to nearly the same line stiffness for both types of nanoribbon (figure 3), and their mechanical flexibility does not change much with the passivation of edges.

3.3. Electronic and carrier transport properties

Next, we calculate the electronic structure of the PNRs considered. The semiconducting behavior of the given PNRs varies from narrow-gap semiconductor ($E_g < 1$ eV) to wide-gap semiconductor ($E_g > 1$ eV). The passivation of edges with hydrogen increases the band gap of PNRs, which lies in the range 0.3–2.2 eV (table 1 and figure 4). The increase in bandgap on the edge passivation is attributed to the pairing of electrons due to hydrogen atoms, which eliminates the

dangling bonds. On passivation, direct ↔ indirect band gap transition has been found to occur in these PNRs. For example, in α_{x1}-PNR, CBM shifts from a point between Γ and X, to Γ, while VBM remains at Γ; in γ_{x1}-PNR, CBM shifts from X to Γ, while VBM remains at Γ; in ϕ_{x1}-PNR, CBM remains at Γ while VBM shifts from X to Γ, leading to an (indirect → direct transition) in these PNRs.

On the other hand, direct → indirect bandgap transition occurs in β_{x1}-PNR due to a shift of CBM from Γ to a point between Γ and X, and of VBM from Γ to X, while in θ_{x1}-PNR and ϕ_{y3}-PNR this transition occurs only due to a shift of CBM from Γ to X, and from Γ to a point between Γ and Y, respectively. The magnitude of the band gap is found to be highly anisotropic, i.e., it is less for a PNR along the *x*-direction than for a PNR along the *y*-direction of same
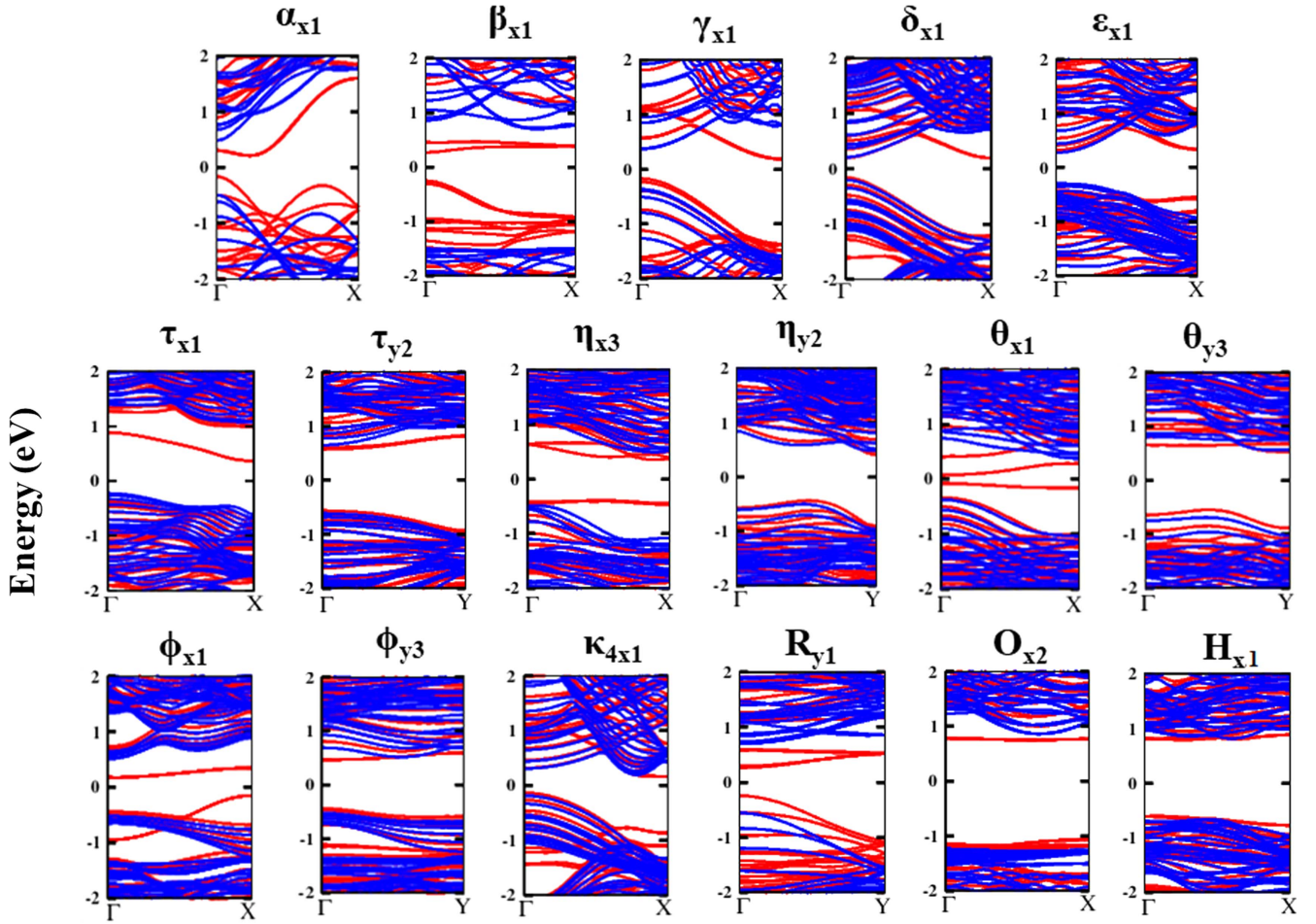
Figure 4. Calculated band structures of phosphorene nanoribbons. Red indicates bands of the bare PNRs while passivated PNRs are shown in blue.

allotrope; for example, the bandgap of τ_{x1} ($E_g = 0.73$ eV) and ϕ_{x1} ($E_g = 0.32$ eV) is respectively less than the bandgap of τ_{y2} ($E_g = 1.14$) and ϕ_{y3} ($E_g = 0.90$). (table 1).

To calculate the carrier mobility, the effective masses of electrons or holes need to be determined (equation (1)). The electron (hole) effective mass is inversely proportional to the curvature of the CBM (VBM) of a given band structure. Therefore, the effective mass of an electron (hole) can be calculated by fitting a small section of the E versus k surface (figure 4) in the vicinity of the CBM (VBM) at zero strain. The calculated results find a large value (2.26 m_e) of the electron effective mass in the bare κ_{4x1}-PNR, which can be attributed to the presence of a flat conduction band (band shown in red at the X-point in figure 4) arising due to the dangling electron of the edge atoms. On passivation with hydrogen atoms, the band due to the dangling electrons disappears, and the CBM possesses a larger curvature which gives rise to a small effective mass (0.04 m_e). The free charge carriers at the edges of unpassivated PNRs become bonded to hydrogen atoms, which effects their effective masses and hence their mobilities.

The calculated carrier effective masses are found to be anisotropic in nature (figure 5). Carrier effective masses of α-PNR ($m_e^* = 0.12$ m_e and $m_h^* = 0.08$ m_e) and R-PNR

($m_e^* = 0.23$ m_e and $m_h^* = 0.08$ m_e) are calculated to be the lowest (close to zero line). The effective masses of most of the PNRs are comparable with α-PNR and R-PNR (figure 5). On passivation, the effective mass of most of the PNRs is found to be less than 0.3 m_e. Note that the carrier mobility is inversely proportional to 3/2 power of the effective mass, hence lower effective mass leads to an increase in the mobility.

Another factor which also determines the carrier mobility is the deformation potential (DP) (equation (1)). DP is calculated by the linear fitting of the valence band edge (VBE)/ conduction band edge (CBE) versus strain surface. The magnitude of DP describes the change in energy of the electronic band with the elastic deformation and, therefore, describes the degree to which the charge carriers interact with phonons. A lower value of DP indicates a weaker electron–phonon coupling in the conduction (valence) band, thereby contributing to an increase in the mobility of electrons (holes) [30]. The values of DP are listed in table 1. Note that the negative DP indicates that the deformation in the band edge will be in the opposite direction on the application of a strain.

We now calculate the carrier mobility using equation (1). Our results find the carrier's mobility of given PNRs to be highly anisotropic, e.g, μ_e (μ_h) of θ_{y3} is 253 (11) times that of
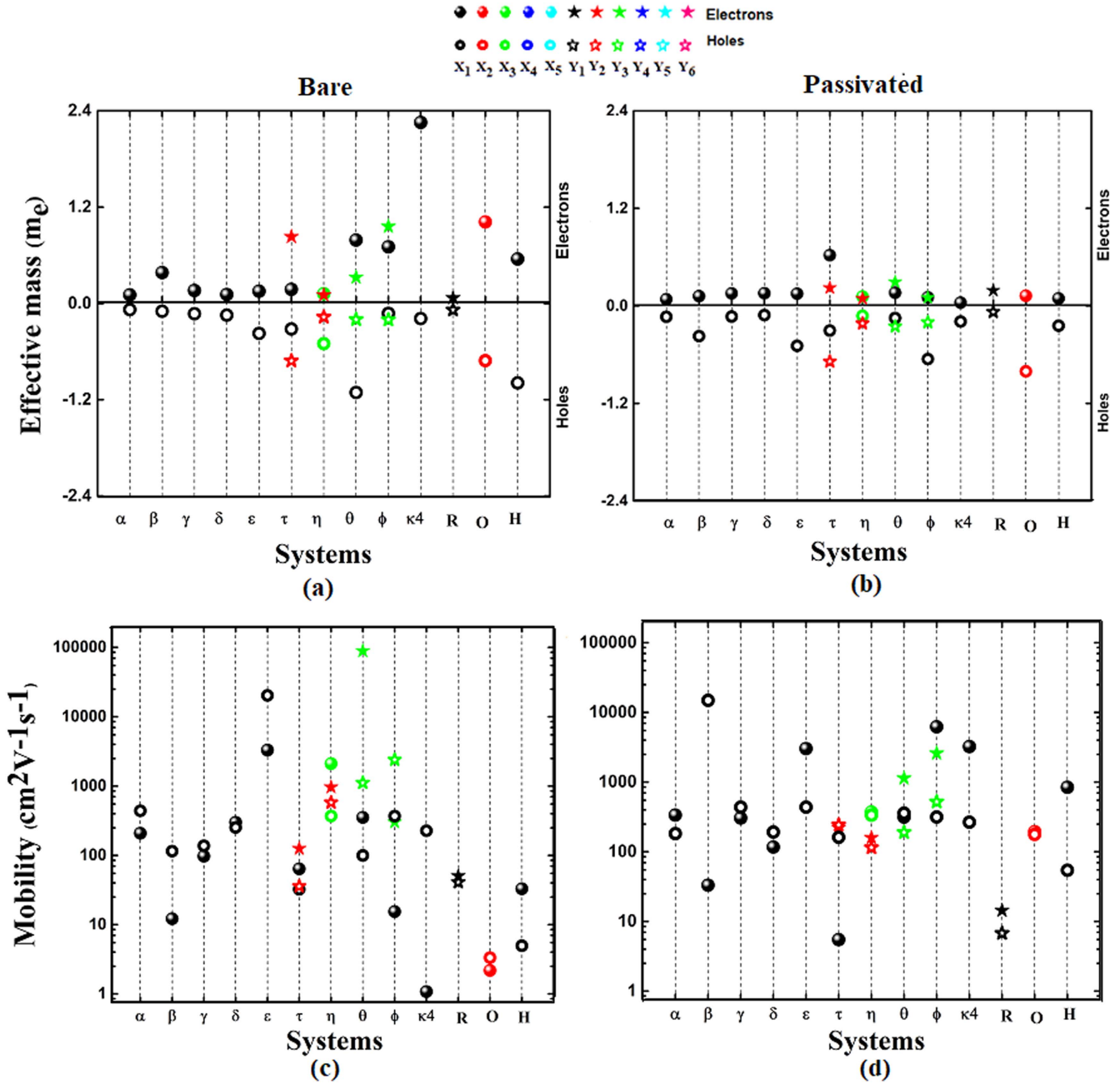
Figure 5. The effective mass and mobility of electrons and holes for bare and passivated PNRs at $T = 300$ K.

μ_e (μ_h) of θ_{x1}, and μ_e (μ_h) of ϕ_{y3} is 20 (7) times that of μ_e (μ_h) of ϕ_{x1}. Note that an anisotropy in the carrier mobility is also reported for black (α) and blue (β) PNRs [7, 19, 31]. It is important to mention here that we have considered a fixed width of PNRs, though the mobility also depends on the width of given ribbons [18, 32]. Although line stiffness remains almost unaffected by the passivation of the edges but the effective masses and deformation potentials show significant modulation that leads to enhancement in the carrier mobility on edge-passivation, e.g., hole mobility in β-PNR increases 130 times and electron mobility in κ_4-PNR increases 3000 times on passivation (figure 5 and table S2).

The carrier mobilities of most of the PNRs considered are found to be comparable to that of monolayer black phosphorene (i.e. 10^3 cm^2 V^{-1} s^{-1}) with the exception of β-PNR, τ-PNR, R-PNR, and H-PNR. In particular, the electron mobility of θ-PNR and the hole mobility of ε-PNR are found to be one order higher than α-PNR (figure 5 and table S1 of ESI). The electron mobility of the passivated PNRs, including α_{x1}, ε_{x1}, η_{y2}, θ_{y3}, ϕ_{x1}, ϕ_{y3}, κ_{4x1}, R$_{y1}$, O$_{x2}$, and H$_{x1}$, is higher than their hole mobility indicating their n-type semiconducting characteristic, whereas β_{x1}, γ_{x1}, δ_{x1}, τ_{x1}, τ_{y2}, η_{x3}, and θ_{x1} behave like p-type semiconductors owing to their higher hole mobility. Among the PNRs considered, α_{x1}, δ_{x1}, ε_{x1}, τ_{x1}, τ_{y2}, η_{x3}, θ_{x1}, ϕ_{x1}, ϕ_{y3}, κ_{4x1} and O$_{x2}$ PNRs change their carrier mobility, thereby, their semiconducting character (n-type $\leftrightarrow$ p-type) after the passivation of the edges with H atoms. Our results indicate that the intrinsic band gap and

high carrier mobility possessed by these PNRs may find various applications in nano- and opto-electronics.

4. Summary

The stability, electronic and mechanical properties of nanoribbons of 13 phosphorene allotropes, namely α-P, β-P, γ-P, δ-P, ε-P, τ-P, η-P, θ-P, ϕ-P, κ_4-P, R-P, O-P and H-P have been investigated. The magnitude of the formation energies of the PNRs considered is found to be comparable to their monolayer counterparts, indicating their ease of formation. Deformation potential theory within the effective mass approximation has been applied to the most stable semiconducting bare and passivated PNRs in order to analyse their carrier transport properties. On the passivation of edges, the band gap increases, along with direct$\leftrightarrow$indirect transition in some cases. The effective mass of most of the PNRs is less than 0.3 m_{e}. The carrier mobility of most of the PNRs is found to be comparable to that of the monolayer α-P. The unique features of the PNRs considered render them favorable 1D materials to be used in applications relating to phosphorene based devices.

Acknowledgments

ORCID iDs

Sumandeep Kaur ⬤ https://orcid.org/0000-0003-2110-7432
Ashok Kumar ⬤ https://orcid.org/0000-0003-3636-0502
Sunita Srivastava ⬤ https://orcid.org/0000-0001-9543-6349
Ravindra Pandey ⬤ https://orcid.org/0000-0002-2126-1985

References

[1] Brent J R, Savjani N, Lewis E A, Haigh S J, Lewis D J and O'Brien P 2014 Production of few-layered phosphorene by liquid exfoliation of black phosphorous *Chem. Comm.* **50** 13338

[2] Das S, Zhang W, Demateau M, Hoffmann A, Dubey M and Roelofs A 2014 Tunable transport gap in phosphorene *Nano Lett.* **14** 5733

[3] Gusmao R, Sofer Z and Pumera M 2017 Black phosphorus rediscovered: from bulk to monolayer *Angew. Chem. Int. Ed.* **56** 8052

[4] Zhang J L *et al* 2016 Epitaxial growth of single layer blue phosphorus: a new phase of two-dimensional phosphorus *Nano Lett.* **16** 4903

[5] Zeng J, Cui P and Zhang Z 2017 Half layer by half layer growth of a blue phosphorene monolayer on a GaN(001) substrate *Phys. Rev. Lett.* **118** 046101

[6] Zhu Z and Tománek D 2014 Semiconducting layered blue phosphorus: a computational study *Phys. Rev. Lett.* **112** 176802

[7] Liu H, Neal A T, Zhu Z, Luo Z, Xu X, Tománek D and Ye P D 2014 Phosphorene: an unexplored 2D semiconductor with a high hole mobility *ACS Nano* **8** 4033

[8] Xiao J, Long M, Zhang X, Ouyang J, Xu H and Gao Y 2015 Theoretical predictions on the electronic structure and charge carrier mobility in 2D Phosphorus sheets *Sci. Rep.* **5** 9961

[9] Sorkin V, Cai Y, Ong Z, Zhang G and Zhang Y W 2016 Recent advances in the study of phosphorene and its nanostructures *Crit. Rev. Solid State Mater. Sci.* **42** 1

[10] Kaur S, Kumar A, Srivastava S and Kumar T 2016 Electronic structure engineering of various structural phases of phosphorene *Phys. Chem. Chem. Phys.* **18** 18312

[11] Guan J, Zhu Z and Tománek D 2014 Phase coexistence and metal insulator transition in few-layer phosphorene: A computational study *Phys. Rev. Lett.* **113** 046804

[12] Wu M, Fu H, Zhou L, Yao K and Zeng X C 2015 Nine new phosphorene polymorphs with non-honeycomb structures: a much extended family *Nano Lett.* **15** 3557

[13] Wang H, Li X, Liua Z and Yanga J 2017 ψ-phosphorene: a new allotrope of phosphorene *Phys. Chem. Chem. Phys.* **19** 2402

[14] Zhao T, He C Y, Ma S Y, Zhang K W, Peng X Y, Xie G F and Zhong J X 2015 A new phase of phosphorus: the missed tricycle type red phosphorene *J. Phys. Condens. Matter* **27** 265301

[15] Li P and Luo W 2016 A new structure of two-dimensional allotropes of group V elements *Sci. Rep.* **6** 25423

[16] Xu M, He C, Zhang C, Tang C and Zhong J 2016 First-principles prediction of a novel hexagonal phosphorene allotrope *Phys. Status Solidi RRL* **10** 563

[17] Liu J, Zhang S, Guo Y and Wang Q 2016 Phosphorus K4 crystal: a new stable allotrope *Sci. Rep.* **6** 37528

[18] Xiao J, Long M, Zhang X, Zhang D, Xu H and Chan K S 2015 First-principles prediction of the charge mobility in black phosphorus semiconductor nanoribbons *J. Phys. Chem. Lett.* **6** 4141

[19] Xiao J, Long M, Deng C-S, He J, Cui L-L and Xu H 2016 Electronic structures and carrier mobilities of blue phosphorus nanoribbons and nanotubes: a first-principles study *J. Phys. Chem.* C **120** 4638

[20] Zhou B, Zhou B, Liu P and Zhou G 2018 The giant stark effect in armchair-edge phosphorene nanoribbons under a transverse electric field *Phys. Lett.* A **382** 193

[21] Zhou B, Zhou B, Zhou X and Zhou G 2017 Even–odd effect on the edge states for zigzag phosphorene nanoribbons under a perpendicular electric field *J. Phys. D: Appl. Phys.* **50** 045106

[22] Zhang X, Li Q, Xu B, Wan B, Yin J and Wan X G 2016 Tuning carrier mobility of phosphorene nanoribbons by edge passivation and strain *Phys. Lett.* A **380** 614

[23] Soler J M, Artacho E, Gale J D, Garcia A, Junquera J, Ordejon P and Portal D S 2002 The SIESTA method for *ab initio* order-N materials simulation *J. Phys. Condens. Matter* **14** 2745

[24] Troullier N and Martins J L 1991 Efficient pseudopotentials for plane-wave calculations *Phys. Rev.* B **43** 1993

[25] Dion M, Rydberg H, Schröder E, Langreth D C and Lundqvist B I 2004 Van der Waals density functional for general geometries *Phys. Rev. Lett.* **92** 246401

[26] Bardeen J and Shockley W 1950 Deformation potentials and mobilities in non-polar crystals *Phys. Rev.* **80** 72

[27] Beleznay F B, Bogár F and Ladik J 2003 Charge carrier mobility in quasi-one-dimensional systems: Application to a guanine stack *J. Chem. Phys.* **119** 5690

[28] Long M Q, Tang L, Wang D, Li Y L and Shuai Z G 2011 Electronic structure and carrier mobility in graphdiyne sheet and nanoribbons: theoretical predictions *ACS Nano* **5** 2593

[29] Long M Q, Tang L, Wang D, Wang L J and Shuai Z G 2009 Theoretical predictions of size-dependent carrier mobility and polarity in graphene *J. Am. Chem. Soc.* **131** 17728

[30] Wang H, Pei Y, LaLonde A D and Snyder G J 2012 Weak electron–phonon coupling contributing to high thermoelectric performance in n-type PbSe *PANS* **109** 9705

[31] Zhang X, Li Q, Wan B, Yin J and Wan X G 2016 Tuning the carrier mobility of phosphorene nanoribbons by edge passivation and strain *Phys. Lett.* A **380** 614

[32] Swaroop R, Ahluwalia P K, Tankeshwar K and Kumar A 2017 Ultra-narrow blue phosphorene nanoribbons for tunable optoelectronics *RSC Advances* **7** 2992